Corrosion Science 100 (2015) 377–385

Contents lists available at ScienceDirect

Corrosion Science

journal homepage: www.elsevier.com/locate/corsci

Effect of sulphate impurity in chromic acid anodizing of aluminium

D. Elabar, A. Němcová, T. Hashimoto, P. Skeldon*, G.E. Thompson

Corrosion and Protection Group, School of Materials, The University of Manchester, Manchester M13 9PL, UK

ARTICLE INFO

Article history:
Received 30 April 2015
Received in revised form 4 August 2015
Accepted 5 August 2015
Available online 10 August 2015

Keywords:
A. Aluminium
B. RBS
B. SEM
B. TEM
C. Anodic films

ABSTRACT

The formation of porous anodic alumina during potentiostatic anodizing of aluminium for times up to 900 s has been investigated using two grades of chromic oxide reagent. The anodic films were examined by ion beam analysis and scanning and transmission electron microscopies. Sulphate impurity in the chromic acid led to incorporation of sulphate into the anodic film, a lower current density, a smaller cell size and less feathering of the pore walls. In addition, the efficiency of film formation was increased. The sulphate concentration in the film was greatly enhanced relative to the electrolyte.

1. Introduction

Anodizing processes are widely used for protecting aluminium alloys against corrosion [1]. The resultant films are composed of amorphous alumina and consist of a relatively thick, porous, outer region and a thinner, non-porous, inner region [2,3]. The porous region contains the major pores of the film, which extend from the film surface to the barrier layer. Near the film surface, shorter, incipient pores are also present, whose growth stopped in the early stages of anodizing. The diameter of the major pores and the thickness of the inner, barrier region are dependent on the potential applied during anodizing, with typical proportionalities of ~1 nm V^{-1} [3,4]. Studies of ionic migration in barrier-type and porous anodic alumina films have usually found a transport number of O^{2-} ions of ~0.6 [5,6]. During the formation of porous films, the outward migrating Al^{3+} ions, constituting the remainder of the ionic current, are ejected to the electrolyte at the pore bases [7]. The electronic current in the barrier region is generally considered to be negligible. The thickness of the barrier region, which is relatively constant during the growth of a film under either a constant potential or constant current density, is maintained by a balance between growth of the barrier layer by continued oxidation of the aluminium substrate and thinning of the barrier layer by either field-assisted dissolution of the alumina at the pore bases [8] or field-assisted flow of alumina from the barrier layer to the pore walls [9–13]. The pores may be widened toward the film surface by chemical dissolution to an extent dependent on the anodizing conditions.

Porous anodic films are most commonly formed in chromic, oxalic, phosphoric and sulphuric acids. The films formed in the last three acids contain anions of the electrolyte and the pore walls are smooth [14,15]. In contrast, the films formed in chromic acid contain comparatively few chromate ions [16–18], and the pore walls are feathered [16] Additionally, the pore arrangement is less orderly compared with films formed in the other electrolytes [18], which can be used as porous alumina templates [19,20]. The contrasts between anodizing in chromic acid and the other acids indicate that significant differences between the anodizing behaviours remain to be understood.

In the present study, the formation of porous anodic films on aluminium in chromic acid is further investigated. The films are industrially important, especially for coating systems for aerospace alloys. Two grades of chromic oxide reagent are compared that differ particularly in the concentrations of sulphate impurity. In addition, arsenic species, which are immobile in anodic alumina [21], are incorporated into the film by pre-anodizing in a sodium arsenate electrolyte to assist the study of the film growth. A similar approach has been used to study pore formation in phosphoric acid [21].The amounts and locations of arsenic and sulphur are determined by a combination of ion beam analysis and transmission electron microscopy. The study shows a significant effect of the sulphate impurity on the growth rate, composition and morphology of the films.

* Corresponding author. Fax: + 44 161 306 4865.
E-mail address: p.skeldon@manchester.ac.uk (P. Skeldon).

http://dx.doi.org/10.1016/j.corsci.2015.08.019

2. Materials and methods

2.1. Specimen preparation

Specimens of dimensions 3 × 1.5 cm were cut from 99.99% aluminium sheet, of 0.3 mm thickness, with a cubic texture. The specimens were first electropolished for 3 min in perchloric acid/ethanol (20:80 by vol.) at 278 K. Following rinsing in ethanol and deionized water, they were masked with lacquer (Stopper 45 MacDermid), leaving a working area of ~3 cm^2 on one side of each specimen, and then anodized to 60 V at a constant current density of 5 mA cm^{-2} in 0.1 mol dm^{-3} sodium arsenate (Fisher Chemical, AR grade: $Na_2HAsO_4.7H_2O$: Cl ≤ 10, N ≤10, S ≤ 50 (ppm)) electrolyte at 293 K. The specimens were removed immediately from the electrolyte at the termination of anodizing, rinsed in deionized water and dried in a flow of cool air.

Following this treatment, a piece was cut from each specimen for ion beam analysis. The remainder of each specimen was re-masked and used for additional anodizing treatments in chromic acid. Some of the specimens were first immersed for 60 s in 0.4 mol dm^{-3} chromic acid at 313 K in order to remove arsenic species that were either adsorbed at the film surface or incorporated into a near-surface film region. The specimens were rinsed and dried as indicated previously and a piece of each specimen was kept for analysis. Other specimens were anodized directly in chromic acid.

Anodizing was carried out at 100 V for times from 15 to 900 s in 0.4 mol dm^{-3} chromic acid at 313 K, followed by rinsing and drying as described previously. For one group of specimens, the chromic oxide reagent used to prepare the electrolyte (Fisher Chemical (AR Grade) contained the following impurities according to the supplier's batch analysis: 0.12 Ca, ≤50 Cl, <0.02 Ce, 48.99 Fe, 11.67 K, 0.48 Mg, 429.44 Na, 2 N, 0.32 P, <0.4 Pb, 314.69 S, 64.68 Si, 0.59 Zn (ppm). The sulphur impurity in the electrolyte is mainly present as sulphate. For the second group, the reagent (Acros Organics (ACS Reagent Grade, 98% purity)) contained the following impurities: Cl ≤50, NO_3^- <500, SO_4^{2-} <50 (ppm). The respective electrolytes are designated HSCA and LSCA, referring to their high and low levels of sulphate, which were ~38 and ≤1.5 ppm, which are equivalent to ~0.39×10^{-3} and <1.6×10^{-5} mol dm^{-3}. The pH and ionic conductivity were 1.062 and 131.71 mS cm^{-1} for HSCA, and 1.083 and 124.2 mS cm^{-1} for LSCA. A series of other electrolytes was prepared using LSCA to which anhydrous sodium sulphate (Na_2SO_4, Merck KGaA, ACS grade) was added. These electrolytes contained up to 150 ppm sulphate. The prior immersion treatments in chromic acid for 60 s for the specimens of the first and second groups employed HSCA and LSCA respectively.

Anodizing was carried out in a two-electrode glass cell containing 500 cm^3 of stirred electrolyte. The cathode was an aluminium sheet with an area of 210 cm^2. The electrolytes were prepared using deionized water; the temperature was controlled using a heater/stirrer unit with a contact thermometer (C-MAG HS 7 digital IKAMAG/ETS-D5). Constant current and constant potential anodizing employed Model 6911 DC and GPR-100H05 power supplies respectively, with recording of the voltage and the current every 0.1 s by a computer with in-house Labview software. The voltages selected for the anodizing treatments in the sodium arsenate and chromic acid electrolytes replicated those of a previous study of pore formation in phosphoric acid [21].

The pore volumes in the porous regions of films were determined using the pore-filling method. Specimens were pre-anodized in the sodium arsenate electrolyte and then re-anodized in either LSCA of HSCA. The pore filling was carried out at 5 mA cm^{-2} in 0.1 mol dm^{-3} ammonium pentaborate electrolyte at 293 K. The porosities were calculated from the slopes of the voltage-time curves [22]. Anodizing of electropolished aluminium to 100 V in the ammonium pentaborate electrolyte under the conditions used for the porosity measurements was also employed to generate barrier-type films, which were then immersed for 60 s in the sodium arsenate electrolyte at 293 K in order to assess the accumulation of arsenic on the film surface due to the immersion treatment.

In order to determine the dissolution rates of the films in the two purities of chromic acid, specimens anodized in the sodium arsenate electrolyte were immersed for times up to 1800 s in either LSCA or HSCA at 313 K. The specimens were then re-anodized at 5 mA cm^{-2} in the sodium arsenate electrolyte. The reduction in voltage between the anodizing and re-anodizing stages was used to calculate the loss of film thickness, based on a formation ratio of 1.2 nm V^{-1} for barrier-type films formed at this current density [23]. The rate of stirring of the LSCA and HSCA solutions used in the immersion treatments and dissolution measurements was the same as that employed in anodizing.

2.2. Specimen examination

The anodized specimens were analysed by Rutherford backscattering spectroscopy (RBS) and nuclear reaction analysis (NRA), using ion beams provided by the Van de Graaff generator at the University of Namur, Belgium. RBS employed 2.0 MeV $^4He^+$ ions, with a scattering angle of 165°. Data analysis used the RUMP program [24]. The arsenic contents of the specimens were determined from the ratio of the yields from arsenic and from bismuth in a reference specimen of bismuth-implanted silicon, assuming Rutherford cross-sections. The statistical error in the individual arsenic peaks was ~3%. NRA employed the $^{16}O(d,p_1)^{17}O$ reaction, using 860 keV $^2H^+$ ions with detection of protons at 150° [25]. The ^{16}O contents of the specimens were determined by comparison with a reference specimen of anodized tantalum. The total oxygen contents of the specimens were corrected for the isotopic abundance of O^{16} (99.8%). The accuracy of the individual analyses was ~3%. The area of the RBS and NRA analyses was ~1 mm^2.

Cross-sections of anodized specimens, of nominal thickness 15 nm, were prepared for transmission electron microscopy (TEM) using a Leica Ultracut microtome with a Micro Star diamond knife. The specimens were then examined either in a JEOL 2000 FX II instrument at an accelerating voltage of 120 kV or a Titan G2 80–200 instrument with ChemiSTEM™ Technology (FEI company), operated at 80 keV. The latter instrument utilizes probe-correction technology and large-solid-angle, windowless, silicon-drift X-ray detectors. Cross-sections of anodized specimens were also examined by scanning electron microscopy (SEM) using a Zeiss Ultra 55 instrument. The cross-sections were prepared by cutting the specimens using a diamond knife and examining the exposed surfaces. In addition, in order to determine the cell sizes, the aluminium substrates were observed following dissolution of the anodic films by immersion for 15 min in a solution containing 20 g l^{-1} CrO_3 and 35 ml l^{-1} of H_3PO_4 (85% w/w) at 333 K.

3. Results and discussion

3.1. Formation of films in sodium arsenate electrolyte and dissolution of the films in chromic acid

The pieces of specimens anodized only in the sodium arsenate electrolyte were analysed by RBS to determine the arsenic contents of films. Table 1 lists the results. Examples of RBS spectra are presented later. The LSCA group contained $4.5 \pm 0.2 \times 10^{15}$ As atoms cm^{-2}, which reduced to 3.8 ± 0.2 As atoms cm^{-2} following immersion for 60 s in LSCA. The respective values for the HSCA group were $4.6 \pm 0.2 \times 10^{15}$ and $3.9 \pm 0.2 \times 10^{15}$ As atoms cm^{-2}. The average arsenic loss for the two groups is ~7×10^{14} As atoms cm^{-2} (a reduction in the initial content by ~15%). Fig. 1 shows the thick-

Table 1
Results of RBS analyses of the arsenic contents of anodic films formed on aluminium to 60 V at 5 mA cm^{-2} in 0.1 mol dm^{-3} sodium arsenate electrolyte at 293 K (Anod.) then immersed in chromic acid at 313 K for 60 s (Imm.) and finally re-anodized at 100 V for different times in 0.4 mol dm^{-3} chromic acid electrolyte at 313 K (Re-anod.). For the HSCA group, analyses were carried out at three locations on each piece of the specimens and the average of the results is recorded. For the LSCA group, one location was analysed. The accuracy of the individual analyses was ±0.3 × 10^{15} As atoms cm^{-2}. (LSCA and HSCA indicate chromic acid containing relatively low and high concentrations of sulphate impurity).

Re-anodizing time	LSCA			HSCA		
(s)	(x10^{15} As atoms cm^{-2})					
	Anod.	Imm.	Re-anod.	Anod.	Imm.	Re-anod.
15	4.6	3.7	3.7	4.3	4.0	3.6
30	4.1	3.4	3.0	4.8	3.7	3.6
90	4.9	4.3	2.7	4.7	4.3	3.6
180	4.7	3.7	2.9	4.5	3.9	3.5
360	4.1	3.9	2.6	4.7	3.8	3.7

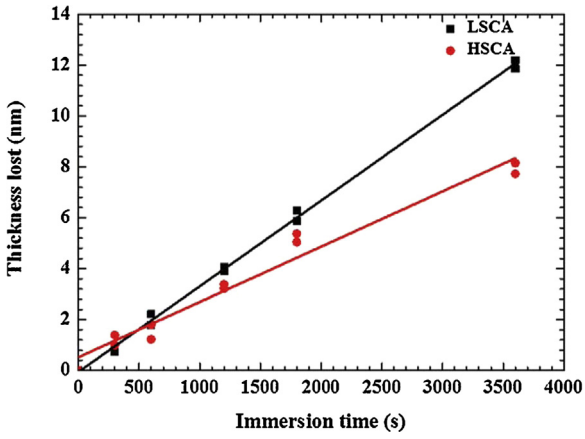

Fig. 1. Dependence of the loss of thickness of anodic films formed on aluminium at 5 mA cm^{-2} to 60 V in 0.1 mol dm^{-3} sodium arsenate electrolyte at 293 K on the time of immersion at the open circuit potential in 0.4 mol dm^{-3} chromic acid at 313 K containing low (LSCA) or high (HSCA) concentrations of sulphate impurity.

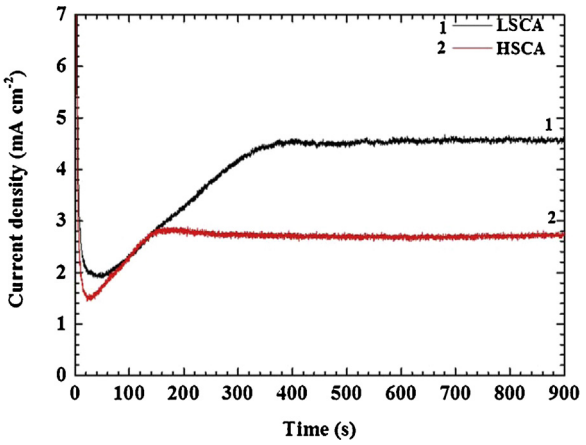

Fig. 2. The dependence of the current density on time during anodizing of aluminium for 900 s at 100 V in 0.4 mol dm^{-3} chromic acid electrolyte at 313 K. The aluminium had been anodized previously at 5 mA cm^{-2} to 60 V in 0.1 mol dm^{-3} sodium arsenate electrolyte at 293 K. Curve (1) low sulphate electrolyte (LSCA). Curve (2) high sulphate electrolyte (HSCA).

ness losses from films formed in the sodium arsenate electrolyte during immersion in LSCA and HSCA; the results indicate dissolution rates of ~3.4 × 10^{-3} and 2.2 × 10^{-3} nm s^{-1} respectively. The oxygen contents of the LSCA and HSCA groups, determined by NRA, were 4.11 ± 0.05 × 10^{17} and 3.85 ± 0.08 × 10^{17} O atoms cm^{-2}. The average value, namely 3.98 × 10^{15} O atoms cm^{-2}, corresponds to a ~72 nm thick film, assuming a film density of 3.1 g cm^{-3}, and a formation ratio of ~1.2 nm V^{-1} [23]. The change in the oxygen content due to the immersion treatment was negligible.

Earlier work has shown that arsenic is located in the outer ~0.40 of the film thickness, i.e a region of ~29 nm thickness, where, in agreement with the present results, the atomic ratio of arsenic to aluminium is ~0.04 [21] According to Fig. 1, the thickness loss due to dissolution of the arsenic-containing alumina for 60 s in LSCA and HSCA is estimated to be ~0.13 and 0.20 nm respectively. Such thicknesses contain ~2–3 × 10^{13} As atoms cm^{-2}, which is much less than the loss due to the immersion treatment. Hence, the latter arises mainly from adsorbed or near-surface-incorporated species. A similar amount of molybdenum and tungsten species have been detected at the surface of barrier-type anodic films formed in molybdate and tungstate electrolytes [26].

A specimen that was anodized in ammonium pentaborate electrolyte to 100 V and then immersed in the sodium arsenate electrolyte for 60 s and rinsed in deionized water accumulated ~2 × 10^{14} As atoms cm^{-2}. The immersion time was ~2.4 times greater than the time required to anodize specimens in the latter electrolyte. The accumulated arsenic is about three times less than the loss following immersion in chromic acid of specimens anodized in the sodium arsenate electrolyte. The higher loss may be due to the influences of the electric field on adsorption of arsenate ions and to differences in the structure and composition of the film surfaces of formed in the ammonium pentaborate and sodium arsenate electrolytes.

3.2. Re-anodizing in chromic acid: current-time response

Fig. 2 shows the dependence of the current density on the time of re-anodizing at 100 V in LSCA and HSCA of specimens pre-anodized to 60 V in the sodium arsenate electrolyte. With both electrolytes, the current density surges to a high value due to rapid film growth, then decreases as the growth rate reduces, and lastly rises to a relatively constant value. Results for shorter times of re-anodizing (listed in Table 1) reproduced closely the relevant parts of the curves of Fig. 2. The minimum current density and plateau value were in the ranges 1.8–2.0 mA cm^{-2} and 4.5–4.6 mA cm^{-2} respectively for LSCA, and 1.3–1.5 mA cm^{-2} and 2.6 –2.9 mA cm^{-2} for HSCA. Thus, the steady current density was increased by a factor of ~1.5–1.8 with LSCA. A small peak in the range ~2.7–3.0 mA cm^{-2} at 150–185 s was also consistently observed for HSCA.

In order to demonstrate the role of sulphate impurity in the chromic acid on the anodizing behaviour, additions of sodium sulphate were made to LSCA. Fig. 3 shows the change in current density-time curves from the LSCA type to the HSCA type as the concentration of sulphate was increased from 15 to 150 ppm. A close match with the HSCA curve occurred with 60 ppm sulphate. Similar results were obtained using additions of sulphuric acid. The results confirm the influence of sulphate ions. In an earlier study, aluminium was anodized galvanostically in mixed sulphuric-chromic acid electrolytes [27,28]. An increase in the amount of sulphuric

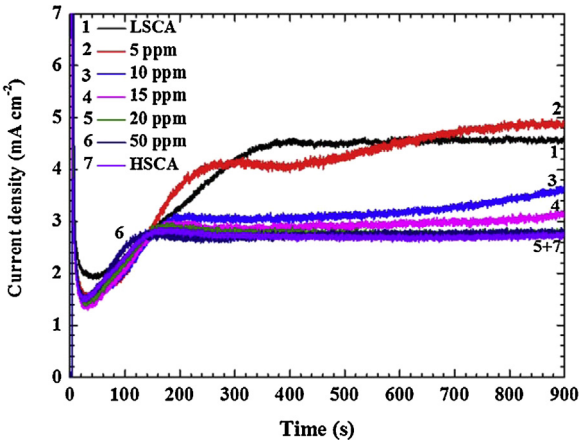

Fig. 3. The dependence of the current density on time during anodizing of aluminium for 900 s at 100 V in 0.4 mol dm^{-3} chromic acid electrolytes at 313 K. The aluminium had been previously anodized at 5 mA cm^{-2} to 60 V in 0.1 mol dm^{-3} sodium arsenate electrolyte at 293 K. Curves are shown for the low sulphate electrolyte (LSCA) and for the same electrolyte with different amounts of added sulphate added as sodium sulphate. A transition in behaviour is evident to that of the high sulphate electrolyte (HSCA).

acid led to a decrease in the potential during the film growth. Under potentiostatic conditions, an increase in the steady current density would be expected, contrary to the present trend. In other work, it has been shown that additions of oxalic acid to chromic acid can reduce the voltage during galvanostatic anodizing of AA 2024 aluminium alloy, and also increase the rate of film growth and the corrosion protection [29]. However, the sulphuric and oxalic additions to the chromic acid in the these studies were much higher than the impurity levels in HSCA and LSCA

3.3. *Re-anodizing in chromic acid: film morphologies and compositions by TEM and SEM*

Fig. 4 presents transmission electron micrographs of cross-sections of films formed in the sodium arsenate electrolyte, then immersed in LSCA for 60 s and re-anodized in LSCA for 15, 30, 90, 180 and 360 s. The films had average total thicknesses of ~153, 169, 201, 263 and 465 nm respectively and barrier layer thicknesses of ~144, 132, 136, 133 and 128 nm. The thicknesses have an accuracy of ~5% due to the often irregular scalloping of the aluminium/film interface and the location of the section with respect to the centre of the pores. Terminated pores are evident in the outer regions of the thicker films and the major pores display the feathered walls typical of chromic acid anodizing [16]. Fig. 5 presents micrographs of HSCA films, revealing total thicknesses of ~142, 161, 197, 294 and 503 nm and barrier layer thicknesses of ~128, 132, 136, 117 and 125 nm. From observations of many sections, less feathering of pore walls was evident in HSCA films.

Fig. 6 presents a transmission electron micrograph and elemental maps of aluminium, oxygen, chromium, arsenic and sulphur for a film re-anodized for 180 s in HSCA. Arsenic is present in the outer ~30 nm of the film thickness and sulphur is distributed part way through the pore walls and to a depth of ~70% of the barrier layer thickness. From measurements repeated three times in different parts of the cross-section, the atomic ratio of S:Al was ~0.018–0.021 in the sulphur-rich region beneath the pores, ~0.005–0.007 in the arsenic-rich layer, and ≤0.002 elsewhere in the film. The amount

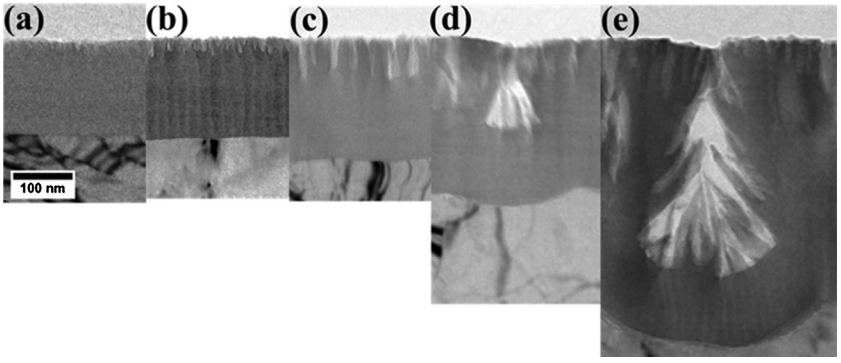

Fig. 4. Bright field transmission electron micrographs of ultramicrotomed cross-sections of aluminium anodized at 5 mA cm^{-2} to 60 V in 0.1 mol dm^{-3} sodium arsenate electrolyte at 293 K, then immersed for 60 s in 0.4 mol dm^{-3} chromic acid at 313 K; and lastly re-anodized for (a) 15 s, (b) 30 s, (c) 90 s, (d) 180 s and (e) 360 s at 100 V in 0.4 mol dm^{-3} low sulphate chromic acid electrolyte (LSCA) at 313 K.

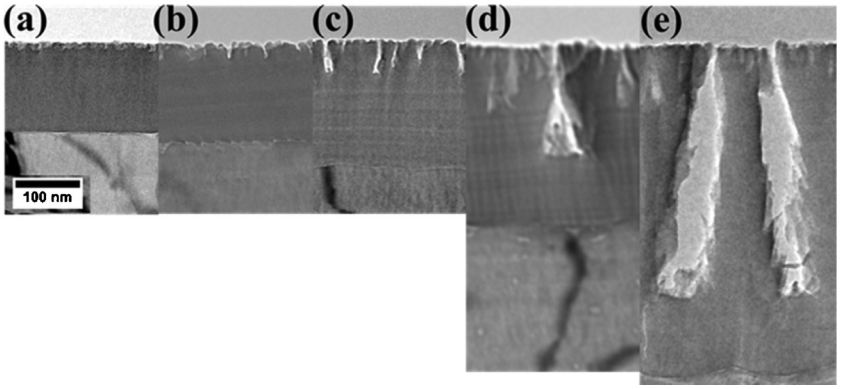

Fig. 5. Bright field transmission electron micrographs of ultramicrotomed cross-sections of aluminium anodized at 5 mA cm^{-2} to 60 V in 0.1 mol dm^{-3} sodium arsenate electrolyte at 293 K and then re-anodized for (a) 15 s (b) 30 s, (c) 90 s, (d) 180 s and (e) 360 s at 100 V in 0.4 mol dm^{-3} high sulphate chromic acid electrolyte (HSCA) at 313 K.

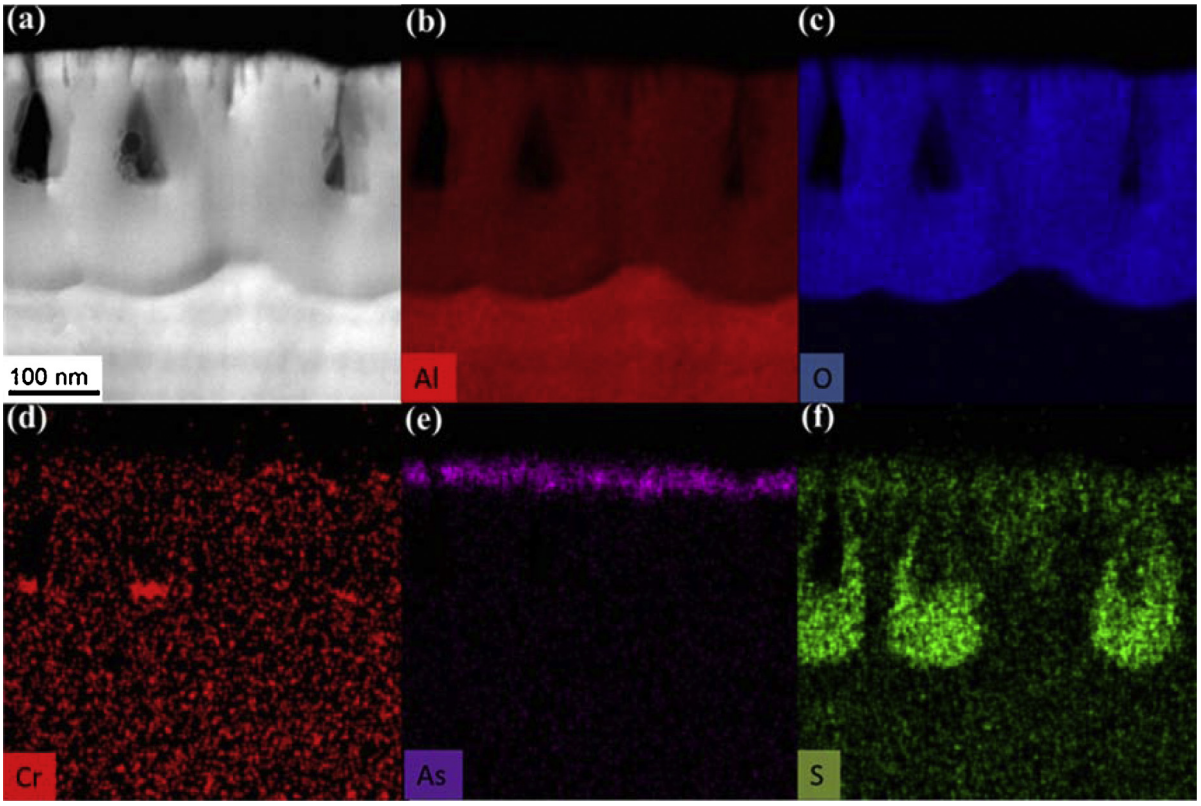

Fig. 6. (a) High angle annular dark field transmission electron micrograph and EDX elemental maps of (b) aluminium, (c) oxygen, (d) chromium, (e) arsenic and (f) sulphur for an ultramicrotomed cross-section of aluminium anodized at 5 mA cm^{-2} to 60 V in 0.1 mol dm^{-3} sodium arsenate electrolyte at 293 K and then re-anodized for 180 s at 100 V in 0.4 mol dm^{-3} high sulphate chromic acid electrolyte (HSCA) at 313 K.

of sulphur incorporated into porous anodic films formed in sulphuric acid increases as the current density is increased [30]. XPS studies have indicated that sulphur is incorporated as sulphate ions [31], which migrate inward in anodic alumina films [32]. The average S:Al ratio in films formed in sulphuric acid depends logarithmically on the current density [15]. The ratio in films formed in 0.4 mol dm^{-3} sulphuric acid at 293 K at 1–3 mA cm^{-2}, i.e. the range for pore formation in HSCA, is ~0.05 [33], whereas the average ratio

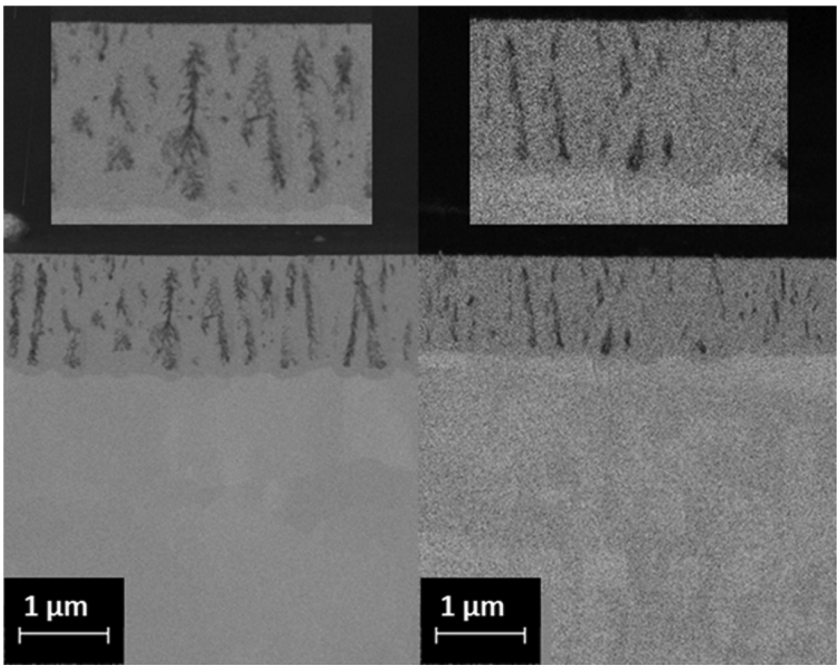

Fig. 7. Scanning electron micrographs (backscattered electrons) of electropolished aluminium anodized at 5 mA cm^{-2} to 60 V in 0.1 mol dm^{-3} sodium arsenate electrolyte at 293 K and re-anodized for 900 s at 100 V in 0.4 mol dm^{-3} chromic acid at 313 K. (a) Low sulphate electrolyte (LSCA). (b) High sulphate electrolyte (HSCA). The insets show the films at increased magnification.

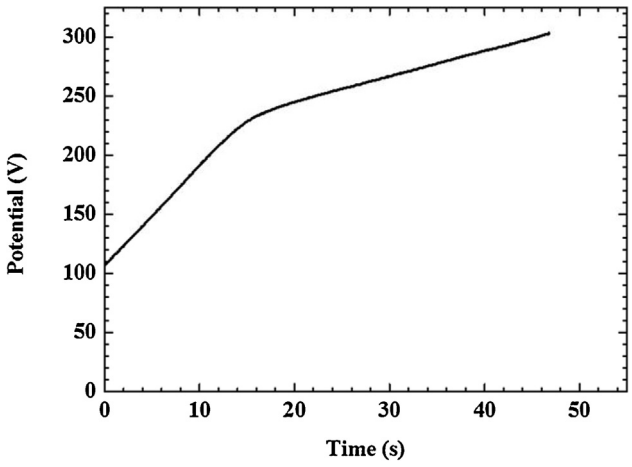

Fig. 8. An example of the voltage-time response during a pore-filling porosity measurement. The aluminium specimen was anodized at 5 mA cm^{-2} to 60 V in 0.1 mol dm^{-3} sodium arsenate electrolyte at 293 K, immersed for 60 s in 0.4 mol dm^{-3} chromic acid at 313 K and then re-anodized for 180 s in 0.4 mol dm^{-3} chromic acid (using low sulphate electrolyte LSCA) at 313 K. The specimen was then further anodized at 5 mA cm^{-2} in 0.1 mol dm^{-3} ammonium pentaborate at 293 K to fill the pores.

in the present film is estimated to be ~0.01. Film crystallization in the TEM has suggested that a sulphur-free region, representing about 5% of the wall thickness, is present at cell boundaries of films formed in sulphuric acid. [14]. However, a recent analytical TEM study was unable to resolve such a boundary region in self-ordered films formed by two-stage anodizing [34]. In the HSCA electrolyte, the molar ratio of sulphur to water molecules, which are the main source of oxygen in the anodic films, is $\sim 7.4 \times 10^{-6}$. The ratio is $\sim 10^3$ times lower than the ratio of S:O in the film, indicating an enhanced incorporation of sulphate relative to the sulphate concentration in the electrolyte. Chromium was detected at some pore bases, which may be due to either species adsorbed during anodizing or residues of the electrolyte that remain after rinsing. EDX analyses of a small, chromium-containing region at a pore base indicated ≤0.2 at.%Cr. Similar elemental maps were obtained for a film formed for 180 s in the LSCA, but no chromium or sulphur was detected.

Fig. 7 compares scanning electron micrographs of cross-sections of specimens that were re-anodized for 900 s in LSCA and HSCA, The respective film thicknesses were 1360 ± 45 and 1132 ± 35 nm. The insets show the films in more detail. The charges passed in the cell during anodizing in LSCA and HSCA were 3775 ± 190 and 2500 ± 125 mC cm^{-2}, which can oxidize 1304 ± 65 and 864 ± 43 nm of aluminium respectively. Following subtraction of the film thickness formed in the sodium arsenate electrolyte, the volume expansions on converting the aluminium to oxide are 0.99 ± 0.06 and 1.23 ± 0.08 respectively. The experiment was twice repeated, yielding volume expansions of 0.99 and 1.03 for LSCA and 1.22 and 1.25 for HSCA.

3.4. Re-anodizing in chromic acid: film porosity and cell size

Fig. 8 shows a typical voltage-time curve for the porosity measurements, using the example of a film formed for 180 s in LSCA, with a ~140 nm thick porous region. The voltage surged to ~108 V due to the previous anodizing in LSCA at 100 V. The voltage difference is due to the differing temperatures and compositions of the electrolytes. The voltage then rises linearly and reduces in slope when the pores are fully filled. The porosities of the LSCA films were 15, 13, 14, 15, 17 and 17 % after re-anodizing for 30, 90, 180, 360, 600 and 900 s respectively. The values for the HSCA films were 20, 11, 12, 13, 13 and 15%. The porosities after re-anodizing for 15 s could not be determined accurately owing to the short time required to fill the pores.

Fig. 9 shows scanning electron micrographs of the specimen surfaces after chemical stripping of the anodic films formed by re-anodizing for 360 s in LSCA and HSCA. Both surfaces reveal irregularly ordered cells of various sizes and shapes. The distribution of cell diameters determined from image analyses are shown in Fig. 10. HSCA resulted in a greater proportion of smaller cells compared with LSCA. The average cell diameters are 137 and 214 nm respectively, corresponding to ratios of ~1.4 and 2.1 nm V^{-1}. The ratio for the HSCA specimen is significantly lower than the usual range of values for porous anodic alumina, namely ~2.0–2.5 nm V^{-1} [3,35]. Other studies have also occasionally reported an apparently anomalous pore and cell size under certain conditions of film growth [36,37].

3.5. Re-anodizing in chromic acid: film analyses by RBS and NRA

Fig. 11 presents RBS spectra for three pieces of two specimens: the pieces were (i) anodized in sodium arsenate electrolyte, (ii) immersed in chromic acid for 60 s and (iii) re-anodized for 360 s in either LSCA (Fig. 11(a)) or HSCA (Fig. 11(b)). The spectra show reduced arsenic peaks following the immersion and re-anodizing treatments. The peak widths were negligibly altered after re-anodizing, which is consistent with a thickness loss of only ~1 nm in 360 s according to Fig. 1. The spectra for other re-anodizing times

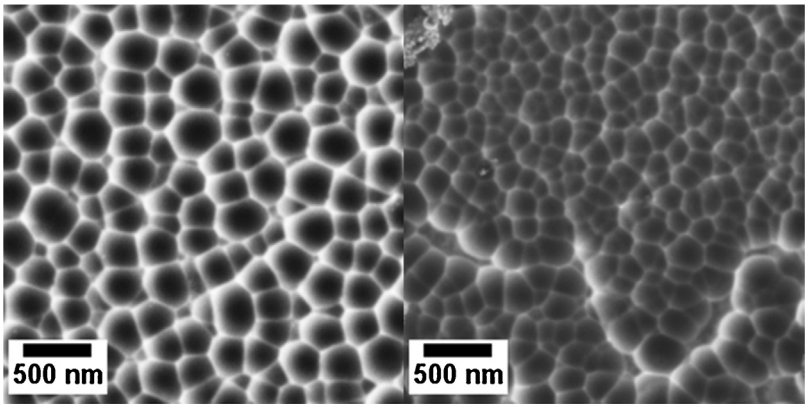

Fig. 9. Scanning electron micrographs (secondary electrons) of the surfaces of aluminium anodized at 5 mA cm^{-2} to 60 V in 0.1 mol dm^{-3} sodium arsenate electrolyte at 293 K, then re-anodized for 360 s at 100 V in (a) 0.4 mol dm^{-3} low sulphate chromic acid electrolyte (LSCA) and (b) 0.4 mol dm^{-3} high sulphate chromic acid electrolyte (HSCA) at 313 K and finally immersed in chromic/phosphoric acid to remove the anodic film.

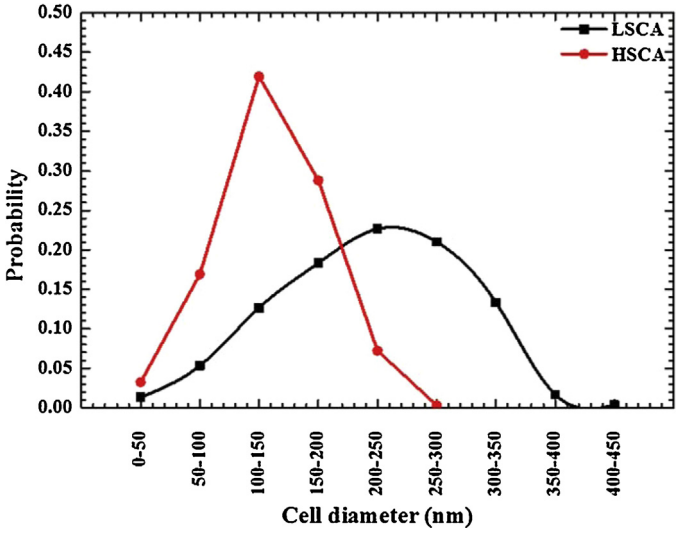

Fig. 10. Distribution of cell diameters determined from the images of Fig. 9.

were generally similar to those presented. Sulphur was detected following re-anodizing in HSCA, with an atomic ratio of S:Al of ~0.01. The analysis depth for sulphur was limited to ~125 nm, due to the overlap of the sulphur and aluminium yields. The S:Al ratio is similar to the estimate obtained from the EDX analysis. No chromium was detected, which indicated an atomic ratio of Cr:Al of $<10^{-3}$. Arrows indicate where chromium at the film surface would be expected to appear. The absence of a significant chromium content agrees with previous work [16,17]. Fig. 11(c) compares the arsenic peak for two pieces of a specimen, one anodized in the sodium arsenate electrolyte the other also immersed in LSCA for 60 s. The pieces were tilted to the He^+ beam in order to increase the depth resolution. The spectra show that arsenic at the film surface of the former piece is removed by the immersion treatment. The arsenic clearly remains near the film surface at the start of re-anodizing when the outward migrating Al^{3+} ions are ejected to the electrolyte. In contrast, re-anodizing in phosphoric acid at 296 K, led to burial of the arsenic beneath a layer of phosphorus-containing alumina [21]. The suppressed ejection of Al^{3+} ions under the latter conditions is possibly to be due to adsorption of phosphate ions and/or their incorporation into the film, or the lower temperature. The anions may reduce adsorption of OH^- ions, which have been proposed to assist ejection of Al^{3+} ions [38] or create a space charge beneath the film surface that retards the ejection of Al^{3+} ions.

The efficiencies of film growth during the re-anodizing process were calculated from the increments in the oxygen content and the charge passed through the cell during time intervals of 30–180 s and 180–360 s. The intervals represent periods of growth mainly of the incipient pores and of the major pores respectively. Earlier times of anodizing were not considered due to the difficulty of obtaining an highly accurate measurement of the cell charge in the period of rapidly changing current and to the initial thickening of the barrier layer that occurred before the initiation of pores. The oxygen contents were measured by NRA; typical NRA spectra have been presented previously [21]. Table 2 presents (i) the thicknesses of aluminium that were oxidized in each time interval, calculated from the charge passed through the cell, assuming formation of Al^{3+} ions, (ii) the thickness of oxide gained according to NRA during re-anodizing, assuming the formation of compact anodic alumina of density 3.1 g cm^{-3}, (iii) the efficiency of film growth and (iv) the ratio of the thickness gain determined from TEM and the thickness of aluminium oxidized, i.e. the volume expansion factor. The efficiency is calculated from the increments in the oxygen contents, with the average charge of oxygen reduced from

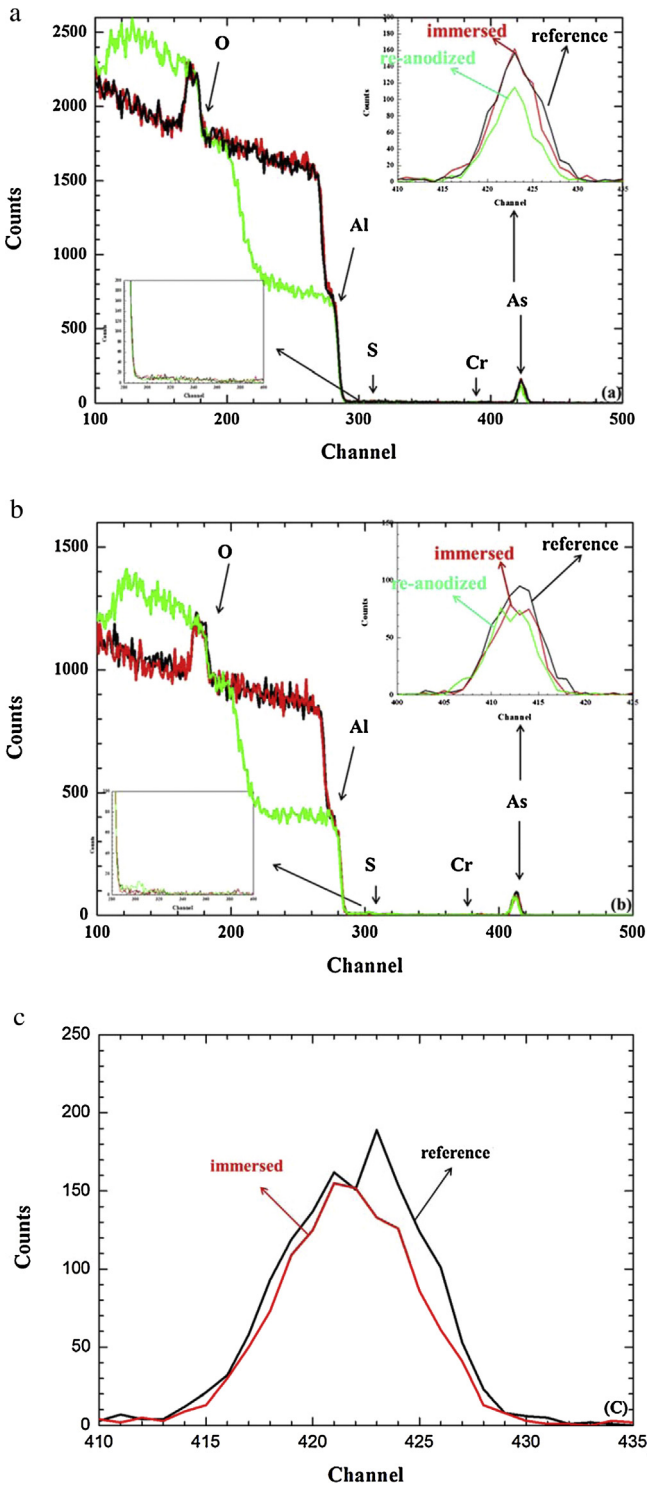

Fig. 11. Comparison of RBS spectra for the three pieces of an anodized aluminium specimen: (i) anodized at 5 mA cm^{-2} to 60 V in 0.1 mol–dm^{-3} sodium arsenate electrolyte at 293 K (labelled reference); (ii) as (i) then immersed for 60 s in 0.4 mol dm^{-3} chromic acid at 313 K; (iii) as (ii) then re-anodized for 360 s at 100 V in 0.4 mol dm^{-3} chromic acid electrolyte at 313 K. (a) Low sulphate electrolyte (LSCA). (b) High sulphate electrolyte (HSCA). (c) Comparison of the arsenic peaks, measured before and after immersion for 60 s in LSCA at 313 K, for a specimen first anodized at 5 mA cm^{-2} –60 V in 0.1 mol dm^{-3} sodium arsenate electrolyte at 293 K. The specimen was tilted to the ion beam in order to increase the depth resolution.

Table 2
Results of RBS and NRA for anodic films were formed to 60 V at 5 mA cm^{-2} in 0.1 mol dm^{-3} sodium arsenate electrolyte at 293 K then immersed in chromic acid at 313 K for 60 s and finally re-anodized at 100 V in 0.4 mol dm^{-3} chromic acid electrolyte at 313 K. (LSCA and HSCA indicate chromic acid containing relatively low and high concentrations of sulphate impurity).

Group	Re-anodizing interval (s)	Increment of charge (mC cm^{-2})	Aluminium oxidized (nm)	Increment of oxygen (x10^{15}atoms cm^{-2})	Oxide gain (nm)	Efficiency of film growth	Expansion factor
LSCA	30–180	319	110.3	485	88.3	0.49	0.85 ± 0.12
	180–360	637	220.2	1017	185.2	0.51	0.92 ± 0.09
HSCA	30–180	330	114.1	636	115.8	0.60	1.17 ± 0.13
	180–360	454	156.9	861	156.8	0.59	1.33 ± 0.13

Table 3
Results of analyses of the arsenic contents of specimens that were re-anodized at 100 V for 50 s in LSCA or HSCA at 313 K respectively and then cut into pieces. The pieces were then immersed in the respective chromic acid at 313 K for different times. The accuracy of the analyses was $\pm 0.2 \times 10^{15}$ and $\pm 0.3 \times 10^{15}$ As atoms cm^{-2} for LSCA and HSCA respectively. (LSCA and HSCA indicate chromic acid containing relatively low and high concentrations of sulphate impurity).

Specimen Immersion time (s)	LSCA (x 10^{15} As at cm^{-2})	HSCA
0	2.5	3.6
15	3.0	3.7
30	2.8	3.7
90	2.8	3.6
180	2.5	3.6
360	2.5	3.5

O^{2-} to $O^{1.95-}$ for HSCA films due to the incorporated sulphate ions. According to Table 2, the efficiencies are ~0.6 and 0.5 in HSCA and LSCA respectively. Additionally, the volume expansion factor for the LSCA films is ~0.9, but increases from ~1.0 to 1.3 for the HSCA films. The incorporated sulphate is expected to have a minor influence on the volume of the film material of ~3%, as estimated from the molecular ratio of $Al_2(SO_4)_3$ and Al_2O_3 in the HSCA films ($\sim 7 \times 10^{-3}$ from the sulphur contents from EDX and RBS analyses) and the Pilling–Bedworth ratios for the respective compounds (6.40 and 1.65).

Table 1 reveals that re-anodizing caused loss of arsenic. There was no correlation of the loss with the re-anodizing time. However, the average loss was 8×10^{14} As atoms cm^{-2} for LSCA and 3×10^{14} As atoms cm^{-2} for HSCA. In order to determine the loss of arsenic due to chemical dissolution during re-anodizing, two specimens were re-anodized in LSCA and HSCA respectively for 50 s. Pores have then passed through the arsenic-containing regions of the films. Pieces of the specimens were immersed for 15, 30, 90, 180 and 360 s in LSCA and HSCA at 313 K, rinsed in deionized water and dried in cool air. RBS results of Table 3 show no significant changes in the amounts of arsenic to an accuracy of $\sim 3 \times 10^{14}$ As atoms cm^{-2}. In comparison, the loss of arsenic from the specimen surface estimated from the dissolution rates derived from Fig. 1 is $\sim 1 \times 10^{14}$ As atoms cm^{-2}. The porosity measurements suggest that ~15% of the arsenic would be lost if pores initiate by a dissolution process, which would equate to $\sim 6 \times 10^{14}$ As atoms cm^{-2}. However, the relatively small measured losses and the accuracy of the measurements preclude a firm conclusion on the mechanism.

The principal findings of the study are that the incorporation of sulphate into the films is associated with a decrease in the current density during formation of the major pores and a change in the morphology of the porous region. The latter undergoes a reduction in the cell size and in the feathering of the pore walls. Further, the volume expansion factor and the efficiency of film growth are increased. The porosity of the film is affected only by a small amount. The decreased current density may arise from increases in the thickness of the barrier layer and/or the ionic resistivity of the film due to the incorporation of sulphate or decrease in the electric field due to space charge. The contrasts between the film growth in LSCA and HSCA indicate an altered growth mechanism due to the presence of sulphate, possibly involving influences of the sulphate on the transport numbers of Al^{3+} and O^{2-} ions [39], the magnitude and distribution of stress, the density of the film material and the sites of new oxide growth. In previous work, the displacement of an arsenic tracer during the formation of a porous film in phosphoric acid suggested that the major pores developed by inward transport of film material, which filled the volume created by the oxidation of the aluminium [21]. Further, stress measurements on films formed in phosphoric acid have revealed a high compressive stress at the film/electrolyte interface, which has been attributed to incorporated phosphate ions [40]. The stress has been proposed to cause oxide flow in the film that generates pores. It has also been suggested that the growth stress can be augmented by residual stress in the substrate that affects the pore population density [41]. It is possible that sulphate ions, generate increased compressive stress and promote oxide flow in the present films. Further, a permanent dipole, due to charges located near the film surface and near the film base, has been detected in anodic alumina films [42]. The former charge was suggested to be associated with electron traps generated by stress from incorporated anions; sulphate ions may have such an influence in the present films. In addition, recent theoretical analysis of film growth has considered that a surface charge may play a role in coupling the reactions at the film surface, such as field assisted ejection of Al^{3+} ions, and the ionic transport within the main body of the film [43]. However, the present results are insufficient to identify clearly the mechanistic influence of the sulphate. In subsequent work, the authors will address this issue further employing tungsten tracers and electrolytes with increased sulphate impurity.

4. Conclusions

1. The rate of film growth during potentiostatic anodizing of aluminium for 900 s at 100 V in 0.4 mol dm^{-3} chromic acid at 313 K is significantly affected by the presence of sulphate impurity in the electrolyte. The steady current density during film growth in an electrolyte containing ~38 ppm sulphate is ~4.6 mA cm^{-2} compared with ~2.8 mA cm^{-2} in an electrolyte containing ≤1.5 ppm sulphate.
2. The reduction in the current density is associated with incorporation of sulphur species into the anodic film, reductions in the mean cell size and in the degree of feathering of pore walls, and increases in the anodizing efficiency and the volume expansion factor. The concentration of sulphur in the film is greatly enhanced compared with the concentration of sulphur impurity and water molecules in the electrolyte.
3. About 7×10^{14} As atoms cm^{-2} are present at the film surface following pre-anodizing of the aluminium in the sodium arsenate electrolyte, which are lost from the film within 60 s of immersion in the chromic acid. The subsequent ejection of Al^{3+} ions from the film to the electrolyte during anodizing in chromic acid has negligible influence on the amount and distribution of arsenic species in the films.

Acknowledgements

The authors thank the Engineering and Physical Sciences Research Council U.K. (LATEST 2 Programme Grant) for support of this work and the European Community for financial assistance within the Integrating Activity "Support of Public and Industrial Research Using Ion Beam Technology (SPIRIT)", under EC contract no. 227012.

References

[1] S. Wernick, R. Pinner, P.G. Sheasby, The Surface Treatment and Finishing of Aluminium and its Alloys, Finishing Publications Limited, Teddington, 1996.
[2] F. Keller, M.S. Hunter, D.L. Robinson, Structural features of oxide coatings on aluminium, J. Electrochem. Soc. 100 (1953) 411–419.
[3] J.P. O'sullivan, G.C. Wood, The morphology and mechanism of formation of porous anodic films on aluminium, Proc. R. Soc. London, Ser. A 317 (1970) 511–543.
[4] G.C. Wood, J.P. O'sullivan, The anodizing of aluminium in sulphate solutions, Electrochim. Acta 15 (1970) 1865–1870.
[5] F. Brown, W.D. Mackintosh, The use of Rutherford backscattering to study the behavior of ion-implanted atoms during anodic oxidation of aluminum: Ar, Kr, Xe, K, Rb, Cs, Cl, Br, and I, J. Electrochem. Soc. 120 (1973) 1096–1102.
[6] C. Cherki, J. Siejka, Study by nuclear microanalysis and O18 tracer techniques of the oxygen transport processes and the growth laws for porous anodic oxide layers on aluminum, J. Electrochem. Soc. 120 (1973) 784–791.
[7] J. Siejka, C. Ortega, An O18 study of field-assisted pore formation in compact anodic oxide films on aluminum, J. Electrochem. Soc. 124 (1977) 883–891.
[8] T.P. Hoar, N.F. Mott, A mechanism for the formation of porous anodic oxide films on aluminium, J. Phys. Chem. Solids 9 (1959) 97–99.
[9] P. Skeldon, G.E. Thompson, S.J. Garcia-Vergara, L. Iglesias-Rubianes, C.E. Blanco-Pinzon, A tracer study of porous anodic alumina, Electrochem. Solid-State Lett. 9 (2006) B47–B51.
[10] J.E. Houser, K.R. Hebert, The role of viscous flow of oxide in the growth of self-ordered porous anodic alumina films, Nat. Mater 8 (2009) 415–420.
[11] K.R. Hebert, S.P. Albu, I. Paramasivam, P. Schmuki, Morphological instability leading to formation of porous anodic oxide films, Nat. Mater. 11 (2012) 162–166.
[12] D. Barkey, J. McHugh, Pattern formation in anodic aluminium oxide growth by flow instability and dynamic recrystallization, J. Electrochem. Soc. 157 (2010) C388–C391.
[13] J. Oh, C.V. Thompson, The role of electric field in pore formation during aluminium anodization, Electrochim. Acta 56 (2011) 4044–4051.
[14] G.E. Thompson, G.C. Wood, Porous anodic film formation on aluminium, Nature 290 (1981) 230–232.
[15] S. Ono, S. Yamashita, N. Masuko, Changes in thickness and degree of anion incorporation of anodic alumina films, in: Proceedings of the Second International Symposium on Aluminium Surface Science and Technology, Manchester, U.K., Benelux Metallurgie, 2000, pp. 163–168.
[16] G.E. Thompson, R.C. Furneaux, G.C. Wood, Electron microscopy of ion beam thinned porous anodic films formed on aluminium, Corros. Sci. 18 (1978) 481–498.
[17] S. Ono, H. Ichinose, T. Kawaguchi, N. Masuko, The observation of anodic oxide films on aluminum by high resolution electron microscopy, Corros. Sci. 31 (1990) 249–254.
[18] W.J. Stepniowski, M. Norek, M. Michalska-Domanska, A. Bombalska, A. Nowak-Stepniowska, M. Kwasny, Z. Boja, Fabrication of anodic aluminium oxide with incorporated chromate ions, Appl. Surf. Sci. 259 (2012) 324–330.
[19] O. Jessensky, F. Muller, U. Gösele, Self-organized formation of hexagonal pore arrays in anodic alumina, Appl. Phys. Lett. 72 (1998) 1173–1175.
[20] K. Nielsch, J. Choi, K. Schwirn, R.B. Wehrspohn, U. Gösele, Self-ordering regimes of porous alumina: the 10% porosity rule, Nano Lett. 2 (7) (2002) 677–680.
[21] A. Baron-Wiecheć, M.G. Burke, T. Hashimoto, H. Liu, P. Skeldon, G.E. Thompson, H. Habazaki, J.-J. Ganem, I.C. Vickridge, Tracer study of pore initiation in anodic alumina formed in phosphoric acid, Electrochim. Acta 113C (2013) 302–312.
[22] H. Takahashi, M. Nagayama, The determination of the porosity of anodic oxide films on aluminium by the pore-filling method, Corros. Sci. 18 (1978) 911–925.
[23] A.C. Harkness, L. Young, High resistance anodic oxide films on aluminium, Can. J. Chem. 44 (1966) 2409–2413.
[24] L.R. Dolittle, Algorithms for the rapid simulation of Rutherford backscattering spectra, Nucl. Instrum. Methods Phys. Res. B 9 (1985) 344–351.
[25] G. Amsel, D. Samuel, Microanalysis of the stable isotopes of oxygen by means of nuclear reactions, Anal. Chem. 39 (1967) 1689–1698.
[26] P. Skeldon, M. Skeldon, G.E. Thompson, G.C. Wood, Incorporation of tungsten and molybdenum species into anodic alumina films, Phil. Mag. B 60 (1989) 513–521.
[27] V.P. Parkhutik, J.M. Albella, Yu E. Makushok, I. Montero, J.M. Martinez-Duart, V.I. Shershulskii, Study of aluminium anodization in sulphuric and chromic acid solutions –I. Kinetcs of growth and composition of oxides, Electrochim. Acta 35 (1990) 955–960.
[28] V.P. Parkhutik, V.T. Belov, M.A. Chernyckh, Study of aluminium anodization in sulphuric and chromic acid solutions –II. Oxide morphology and structure, Electrochim. Acta 35 (1990) 961–966.
[29] V. Moutarlier, M.P. Gigandet, J. Pagetti, B. Normand, Influence of oxalic acid addition to chromic acid on the anodising of Al 2024 alloy, Sur. Coat. Technol. 182 (2004) 117–123.
[30] R.B. Mason, Factors affecting the formation of anodic oxide coatings in sulphuric acid electrolytes, J. Electrochem. Soc. 102 (1955) 671–675.
[31] J.A. Treverton, N.C. Davies, XPS studies of dc and ac anodic films on aluminium formed in sulphuric acid, Electrochim. Acta 25 (1980) 1571–1576.
[32] K. Shimizu, H. Habazaki, P. Skeldon, G.E. Thompson, G.C. Wood, Migration of sulphate ions in anodic alumina, Electrochim. Acta 45 (2000) 1805–1809.
[33] F. Zhou, A.K. Mohamed Al-Zenati, A. Baron-Wiecheć, M. Curioni, S.J. Garcia-Vergara, H. Habazaki, P. Skeldon, G.E. Thompson, Volume expansion factor and growth efficiency of anodic alumina formed in sulphuric acid, J. Electrochem. Soc. 158 (2011) C202–C214.
[34] L. González-Rovira, M. López-Haro, A.B. Hungria, K. El Amrani, J.M. Sánchez-Amaya, J.J. Calvino, F.J. Botana, Direct sub-nanometer scale electron microscopy analysis of anion incorporation to self-ordered anodic alumina layers, Corros. Sci. 52 (2010) 3763–3773.
[35] Y. Li, Y. Qin, S. Jin, X. Hu, Z. Ling, Q. Liu, J. Liao, C. Chen, Y. Shen, L. Jin, A new self-ordering regime for fastproduction of long-range ordered porous anodic aluminium oxide films, Electrochim. Acta 178 (2015) 11–17.
[36] A. Mozalev, A. Poznyak, I. Mozaleva, A.W. Hassel, The voltage-time behaviour for porous anodizing of aluminium in a fluoride-containing oxalic acid electrolyte, Electrochem. Commun. 3 (2001) 299–305.
[37] G. Knörnschild, A.A. Poznyak, A.G. Karoza, A. Mozalev, Effext of the anodization conditions on the growth and volume expansion of porous alumina films in malonic acid electrolyte, Sur. Coat. Technol. 275 (2015) 17–25.
[38] T. Våland, K.E. Heusler, Reactions at the oxide-electrolyte interface of anodic oxide films on aluminium, J. Electroanal. Chem. 149 (1983) 71–82.
[39] K.R. Hebert, J.E. Houser, A model for coupled electrical migration and stress-driven transport in anodic oxide films, J. Electrochem. Soc. 156 (2009) C275–C281.
[40] Ö.Ö. Çapraz, P. Shrotriya, P. Skeldon, G.E. Thompson, K.R. Hebert, Role of oxide stress in the initial growth of self-organized porous aluminium oxide, Electrochim. Acta 167 (2015) 404–411.
[41] M.W. Liao, C.K. Chung, The role and effect of residual stress on pore generation during anodization of aluminium thin films, Corros. Sci. 74 (2013) 232–239.
[42] J. Lambert, C. Guthmann, C. Ortega, M. Saint-Jean, Permanent polarization and charge injection in thin anodic alumina layers studied by electrostatic force microscopy, J. Appl. Phys. 91 (2002) 9161–9169.
[43] S. DeWit, K. Thornton, Model for Anodic film growth on aluminum with coupled bulk transport and interfacial reactions, Langmuir 30 (2014) 5314–5324.